MÜHENDİSLİK ve DOĞA BİLİMLERİ FAKÜLTESİ

**Uluslararası Mühendislik Araştırma ve Geliştirme Dergisi**
**International Journal of Engineering Research and Development**

UMAGD, (2024) 16(2), 707-720.

**10.29137/umagd.1385551**

**Cilt/Volume:16 Sayı/Issue:02 Haziran/June 2024**

Araştırma Makalesi / Research Article

# Dynamic Compression Behavior Of AISI 4340 Steel Under Various Strain Rates And Temperatures

## AISI 4340 Çeliğinin Farklı Gerinme Hızlarında ve Sıcaklıklarda Dinamik Basma Davranışı

**Hakan Hafızoğlu**[1]

[1]*TUBITAK Defense Industries Research and Development Institute, P.K. 16 06261 Mamak Ankara, Turkey*

***Başvuru/Received**: 03/11/2023* ***Kabul / Accepted**: 04/05/2024* ***Çevrimiçi Basım / Published Online:** 30/06/2024*

***Son Versiyon/Final Version**: 30/06/2024*

**Abstract**

In this study, dynamic compression behavior of AISI 4340 steel alloy was investigated with split-Hopkinson and Taylor impact tests and numerical studies. Dynamic compression tests at strain rates of 725, 1500, 2000 $s^{-1}$ at room temperature and at high temperatures of 150 and 250 °C were done using split-Hopkinson pressure bar. Taylor impact tests with the impact velocities of 245, 324 and 336 $ms^{-1}$ were performed with cylindirical specimens to observe dynamic deformation behavior at impact conditions. Numerical studies using Ls-Dyna 3D finite element method were conducted to investigate temperature and stress distribution of specimens during Taylor impact tests. Experimental results revealed that as strain rate increased, yield and ultimate compressive strengths and total strains increased at room temperature at dynamic compression tests. At elevated test conditions, both strengths decreased and total strains increased due to softening effect. Taylor impact test results showed that all the specimens exhibited mushroomed deformation and increase of impact velocity led to shear crack and fracture at the end of deformation process. Numerical results indicates that highest temperatures were obtained at the impact surfaces for three impact velocities. In addition, the increase of impact velocity enhanced the stress distribution at deformed regions near impact surfaces.

**Keywords**

*"Taylor impact test, split-Hopkinson pressure bar, AISI 4340 steel"*

**Öz**

Bu çalışmada, AISI 4340 çelik alaşımının dinamik basma davranışı ayrık-Hopkinson ve Taylor çarpma testleri ve nümerik çalışmalarla incelenmiştir. Ayrık-Hopkinson basınç barı kullanılarak oda sıcaklığında 725, 1500, 2000 $s^{-1}$ gerinme hızlarında ve 150 ve 250 °C yüksek sıcaklıklarında dinamik basma testleri yapılmıştır. Çarpma koşullarında dinamik deformasyon davranışını gözlemlemek için 245, 324 ve 336 $ms^{-1}$ çarpma hızlarında Taylor çarpma testleri icra edilmiştir. Taylor çarpma testlerinde numunelerdeki gerilme ve sıcaklık dağılımının incelenmesi için Ls-Dyna 3D sonlu elemanlar yöntemi kullanılarak numerik çalışmalar yapılmıştır. Deneysel sonuçlar oda sıcaklığında yapılan dinamik basma testlerinde gerinme hızının artışı ile akma ve en fazla basma dayanımının ve toplam gerinmenin arttığını göstermiştir. Yüksek sıcaklık koşullarında yumuşama etkisi dolayısıyla her iki dayanım da düşmüş ve toplam gerinmeler artmıştır. Taylor çarpma test sonuçları tüm numunelerin mantarlanma deformasyonuna uğradığını ve çarpma hızı artışının kesme çatlakları ve deformasyon sürecinin sonunda kırılmaya neden olduğunu göstermiştir. Nümerik sonuçlar en yüksek sıcaklıkların üç çarpma hızı için de çarpma yüzeylerinde bulunduğunu göstermiştir. Ek olarak, çarpma hızının artışı çarpma yüzeylerine yakın deforme olmuş bölgelerde gerilme dağılımını artırmıştır.

**Anahtar Kelimeler**

*"Taylor çarpma testi, ayrık-Hopkinson basıç barı, AISI 4340 çeliği"*

***Responsible Author: hakan.hafizoglu@tubitak.gov.tr**

## 1. Introduction

AISI 4340 is a steel alloy widely used in defense, nuclear, automotive and aerospace industries owing to combination of its high strength, toughness, processability and welding properties (Mahrabi et al., 2020; Souza et al., 2022). Therefore, investigation of deformation behavior of this steel at various strain rates especially in dynamic conditions is so crucial for such industries.

There are some experimental methods to assess the dynamic deformation behaviors of metals in compression direction such as split-Hopkinson pressure bar for strain rates of $10^2$-$10^4$ $s^{-1}$ (Ramesh, 2008) and Taylor impact tests for strain rates of $10^4$-$10^5$ $s^{-1}$ (Campagne et al., 2008). Among those test methods, Taylor impact test is especially preferred to investigate deformation mode of materials with different hardness at various impact velocities which correspond to various strain rates. There have been five different deformation and fragmentation modes reported in the current literature (Xiao et al., 2010; Rakvag et al., 2014). These modes are (i) mushrooming deformation without any crack at impact region (ii) tensile splitting at impact surface of specimen owing to tensile strains which are higher than material ductility (iii) shear cracking owing to high shear stresses (iv) petalling which might occur at high impact velocities for ductile materials and (v) fully fragmentation for brittle specimens. In the literature, there have been experimental and numerical studies related to Taylor impact for steel alloys. Xiao et al. (Xiao et al., 2010) performed Taylor impact tests using 38CrSi steel alloy specimens with varying hardness. The impact velocities in the tests were in the range of 200-600 $ms^{-1}$. They observed mushrooming and shear fracture for all hardness at low impact velocities and petalling fracture for the specimen with low hardness and fragmentation for the specimen with high hardness at high impact velocities. Rakvag et al. (Rakvag et al., 2014) conducted Taylor impact tests with Arne tool steels with different hardness. They observed different fracture modes depending on hardness. Teng et al. (Teng et al., 2005) simulated deformation behavior of Weldox 460 E steel and compared the results with Taylor impact test. Kumar ve Dixt (Kumar and Dixt, 2017) numerically investigated deformation behavior of steel alloy Taylor impact specimens using Abaqus software. They observed no fracture for the impact velocity of 250 $ms^{-1}$ whereas they obtained fractures for the impact velocity of 350 $ms^{-1}$.

Chakraborty et al. (Chakraborty et al., 2015) determined material model parameters by inverse methods for 4340 steel comparing Taylor impact test and numerical results. Acosta et al. (Acosta et al., 2016) found material parameters of AISI 1010 steel by inverse analysis of Taylor impact test. To do this, they compared hardness along the axis of the specimen at numerical and experimental studies.

Sen et al. (Sen et al., 2020) simulated deformation histories of 4340 steel rods for three Taylor impact cases and compared the final dimensions using Johnson-Cook and Zerilli-Armstrong material models. In that study, material parameters of the specimen were determined via inverse formulation (Extended Kalman Filter).

Split-Hopkinson pressure bar has been used commonly to measure dynamic compression behavior of materials (Ramesh, 2008). In the open literature, some studies for measuring dynamic compression behavior of AISI 4340 steel have been reported using split-Hopkinson pressure bar by several researchers (Odeshi et al., 2006; Owolabi et al., 2013; Odoh et al., 2013). In those studies, compression behavior of AISI 4340 steel specimens were investigated at room temperature. No additional tests were done to consider the effect of elevated temperature on mechanical behavior of specimens.

According to literature survey, there have been few studies which investigate dynamic compression behavior of 4340 steel in a wide range of strain rate ($10^2$-$10^5$ $s^{-1}$) at room and elevated temperatures with the combination of split-Hopkinson pressure bar and Taylor impact tests. One of these studies was performed by Piao et al. (Piao et al., 2016). They conducted tests with 4340 steel specimens in the range of $10^{-3}$-$10^6$ $s^{-1}$ in the temperature range of 25-200 °C. In their study, tensile tests were done from quasistatic condition to $10^3$ $s^{-1}$ and Taylor impact tests at impact velocities of 200, 253 and 305 $ms^{-1}$ were done to observe deformation behavior of the specimens. To the author's best knowledge, there have been no comprehensive studies which investigate dynamic compression and fracture behavior of AISI 4340 steel in the range of $10^2$-$10^5$ $s^{-1}$ by experimental and numerical studies. This study focuses on the investigation of dynamic compression and fracture behavior of AISI 4340 steel alloy at various strain rates and temperatures by dynamic compression tests and Taylor impact tests and Taylor impact numerical studies.

## 2. Experimental

AISI 4340 steel was used to determine Johnson-Cook strength model parameters and to perform dynamic tests. In this context, quasistatic tensile tests and dynamic compression tests at various temperatures using split-Hopkinson pressure bar were conducted. Taylor impact tests were done at three impact velocities using single stage gas gun.
Prior to dynamic tests, quasistatic tensile tests (Proline, Zwick/Roell) were done with dog-bone specimens machined according to ASTM-E8 (ASTM E8) to determine Johnson-Cook strength model parameters (A, B, n and C) at strain rates of 0.001, 0.01, 0.1 $s^{-1}$. At least two specimens were tested to ensure the repeatability of each test condition. The quasistatic tensile test specimen geometry is shown in Figure 1.

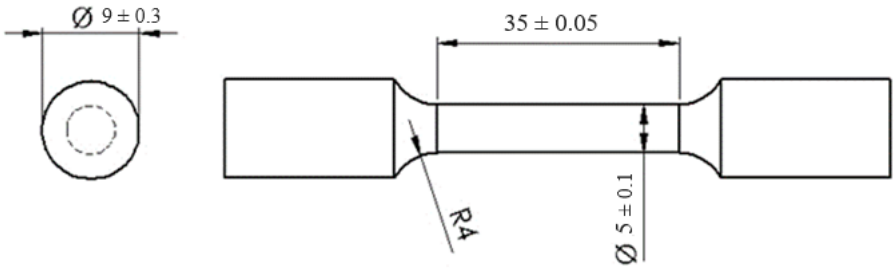


**Figure 1.** Dimensions of quasistatic test specimen.

Dynamic compression tests were performed to determine Johnson-Cook strength model parameters (C and m) and to investigate dynamic deformation behavior and variation of mechanical properties of the alloy by using split-Hopkinson pressure bar. These tests were done with cylindrical specimens with a length and diameter of 6 mm at three strain rates of 725, 1500, 2000 $s^{-1}$ at room temperature and at two elevated temperatures of 150 °C and 250 °C at a fixed strain rate of 725 $s^{-1}$. The dimension and aspect ratio of dynamic cylindrical specimens were specified according to (Chen and Song, 2010). Two tests were performed for each test condition to be sure about the repeatability. Schematic view of test setup is shown in Figure 2.

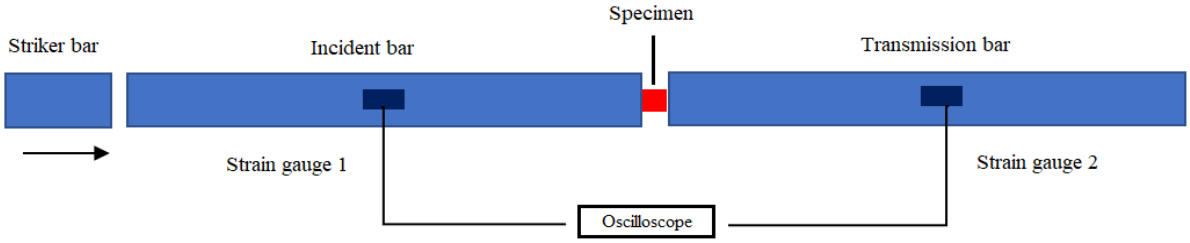


**Figure 2.** Schematic view of split-Hopkinson Pressure bar.

After the impact of striker bar to the incident bar the stress wave propagated along incident bar, specimen and the transmission bar with a speed of sound. Strain gauges captured the signals during wave propagation. These signals were used to determine stress, strain and the strain rate of the compressed specimen using the equations given below (Chen and Song, 2010):

$$\sigma_s = \left(\frac{E_b A_b}{A_s}\right)\varepsilon_T \tag{1}$$

$$\varepsilon_s = -\frac{2c_0}{l_0}\int_0^t \varepsilon_r \, dt \tag{2}$$

$$\dot{\varepsilon}_s = -\frac{2c_0}{l_0}\varepsilon_r \tag{3}$$

where $A_b$ is the cross-sectional area and $E_b$ is the Young Modulus of the bars. $A_s$ and $l_0$ are the initial area and length of the specimen, respectively; $\varepsilon_T$, $\varepsilon_r$ are the strains for transmitted and reflected bars, respectively. $c_0$ is the elastic wave velocity of the bar material.
Taylor impact test specimens were machined with a diameter and length of 8 mm and 24 mm respectively. Taylor impact tests were performed with the impact velocities of 245, 324 and 336 $ms^{-1}$ by using single stage gas gun. Schematic view of test setup for Taylor impact tests is illustrated in Figure 3. In this setup, the specimens were accelerated by means of pressured nitrogen gas in gas gun. After the specimens exited the gun barrel, the velocities were measured by optical device located in the chamber. With a free flight of specimens in a trajectory, the specimens hit the rigid target in front of the gun barrel in the chamber and experienced a plastic deformation. The deformed specimens were scanned by using optical scanning machine to compare the test geometries with numerical ones.

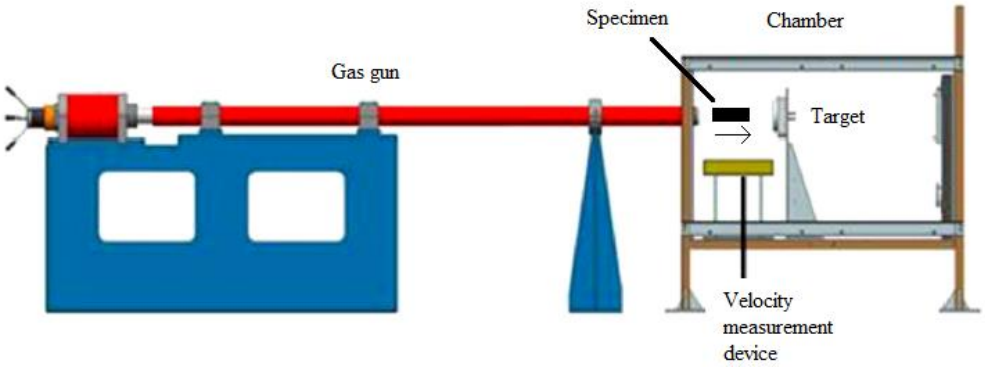


**Figure 3.** Schematic view of Taylor impact test setup.

## 3. Numerical Modeling

Numerical studies were conducted by Ls-Dyna software with Explicit 3-D finite element methods. In the first part of numerical studies, a mesh dependency study was carried out with Taylor impact test analysis to eliminate element size effect on the result. The specimen impacted with 245 $ms^{-1}$ was chosen for this study. Only the element size of the specimen was altered, and the element size of rigid target stayed the same ($0.5 \times 0.5 \times 0.5$ $mm^3$). Element sizes specified in mesh study are $1 \times 1 \times 1$ $mm^3$ with 241536 elements, $0.5 \times 0.5 \times 0.5$ $mm^3$ with 252240 elements, $0.25 \times 0.25 \times 0.25$ $mm^3$ with 337920 elements, $0.125 \times 0.125 \times 0.125$ $mm^3$ with 1023360 elements in the entire model.

After deciding the suitable element size, Taylor impact tests with three impact velocities were modelled to investigate the deformation behavior of the alloy. In Figure 4, Taylor impact test with a rigid target and a steel specimen with an initial velocity was modelled.

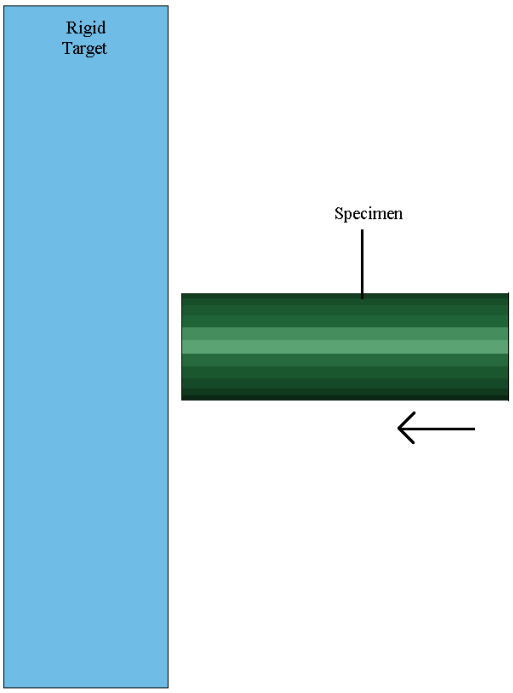


**Figure 4.** FEM model for Taylor impact test.

In numerical modeling studies 15-Johnson_Cook for AISI 4340 alloy and 20-Rigid for target were used as material models. Gruneisen equation of state for steel specimen was assigned in the model. The contact type used in the simulations were set to be Eroding_Surface_to_Surface. The boundary condition identified for the target was Spc_Set. The velocity for Taylor impact specimen was modelled with Velocity_Generation.

Johnson-Cook strength model is generally used for modeling of metals at wide range of strain rates and temperatures (Johnson and Cook, 1983). This model is given as follows:

$$\sigma = (A + B\varepsilon^{n})(1 + C\ln\frac{\dot{\varepsilon_p}}{\dot{\varepsilon_0}})(1 - T^{*m}) \quad (4)$$

where A is the yield stress at reference strain rate and reference temperature, B and n are the parameters related to strain hardening, C is the parameter related to strain rate dependency and m is the parameter corresponding to temperature dependency T* is the homologous temperature given as,

$$T^* = \frac{T - T_{ref}}{T_m - T_{ref}} \quad (5)$$

Here, T is the temperature, $T_{ref}$ is the reference temperature and $T_m$ is the melting temperature of the alloy.
Failure of the steel specimen during impact was also modeled using Johnson-Cook failure model (Johnson and Cook, 1985). The equation of this failure model is expressed as,

$$\varepsilon^f = (D_1 + D_2 \exp(D_3 \sigma^*)(1 + D_4 \ln \frac{\dot{\varepsilon_p}}{\dot{\varepsilon_0}})(1 + D_5 T^*) \quad (6)$$

where the parameters $D_1$-$D_5$ are the empirical parameters which are calculated according to test data, $\varepsilon^f$ is the strain to fracture, $\dot{\varepsilon_p}$ is plastic strain rate and $\dot{\varepsilon_0}$ is reference strain rate.

## 4. Results And Discussion

### 4.1 Experimental Results

*4.1.1.Quasi-static tensile test results*

In Figure 5, quasistatic tensile test results are given for three strain rates. As can be seen from the graph, the increase of strain rate from 0.001 $s^{-1}$ to 0.01 $s^{-1}$ and to 0.1 $s^{-1}$ led to a total increase of yield stress about % 6. However, as the strain rate increased the hardening of the specimens led to more brittle behavior with a result of lower fracture strain. The graphs also showed that all specimens possessed strain hardening behavior up to ultimate tensile strength and strain softening behavior after ultimate tensile strength which might be the result of necking.

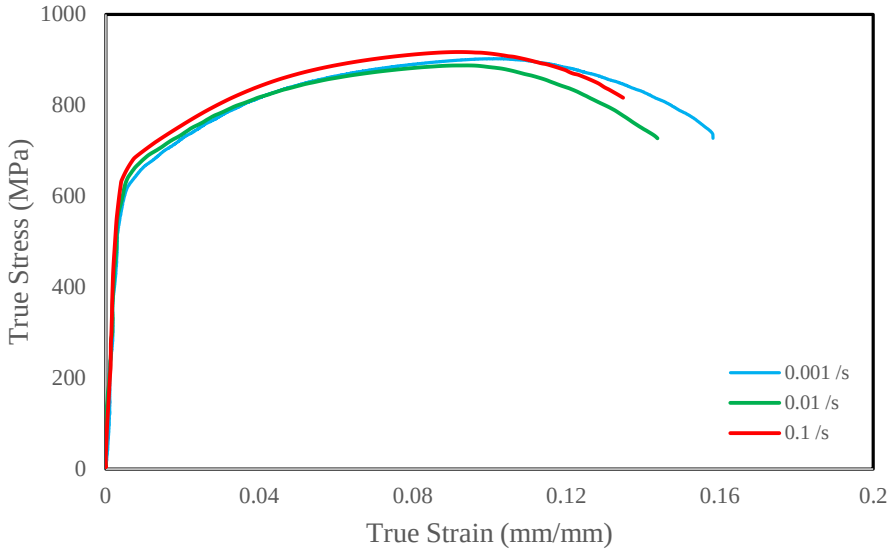


**Figure 5.** Quasistatic tensile test results.

*4.1.2.Split-Hopkinson pressure bar test results*

In Figure 6, the alterations of yield and ultimate compressive strengths and total strains with strain rates are given for room temperature test conditions for split-Hopkinson pressure bar tests. As strain rate increased from 725 $s^{-1}$ to 1500 $s^{-1}$ and from 1500 $s^{-1}$ to 2000 $s^{-1}$, yield strength and ultimate compressive strength increased. Yield strengths were determined in the range of 684-803 MPa. Strain rate increase from 725 $s^{-1}$ to 1500 $s^{-1}$ led to increase of yield strength about 13 % and as the strain rate increased from 1500 $s^{-1}$ to 2000 $s^{-1}$ yield strength increased nearly % 4. Ultimate compressive strengths showed the same increment trend as yield strengths from 942-1075 MPa which was about 14 %. These increases for ultimate compressive strengths were % 9 and % 5 for the strain rate increase from 725 $s^{-1}$ to 1500 $s^{-1}$ and from 1500 $s^{-1}$ to 2000 $s^{-1}$ respectively. These lower increases of yield and ultimate compressive strengths from 1500 $s^{-1}$ to 2000 $s^{-1}$ compared to the increase from 725 $s^{-1}$ to 1500 $s^{-1}$ might be due to more heat occurring at the specimen with

more excessive deformation at higher strain rates. As the total strains were investigated, the increase of strain rate led to increase of total strains about 146 %. Odeshi and Bassim (Odeshi and Bassim, 2009) investigated dynamic deformation and fracture behavior of quenched and tempered AISI 4340 steel. They reported that the yield strengths and tensile strengths were in the range of 1365-1860 MPa and 1500-1980 MPa according to the tempering temperature respectively. Those strengths reported in that study were higher compared to the strengths in current study. This variety might be due to the heat treatments (quenching + tempering) applied to the specimens in the study by Odeshi and Bassim.

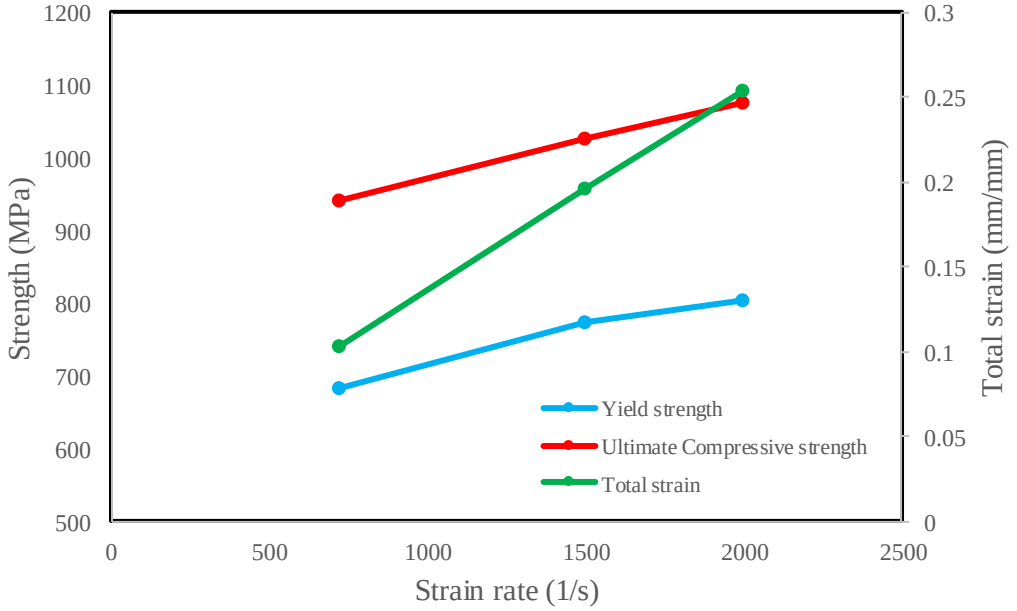


**Figure 6.** The change of strengths and total strains with strain rate.

The effects of dynamic compression temperature on the strengths and total strains after split-Hopkinson pressure bar tests are shown in Figure 7. These high temperature tests were done at a fixed strain rate of 725 $s^{-1}$ to evaluate only the temperature effect on mechanical properties. As temperature increased from room temperature to 250 °C, the yield strength decreased from 684 MPa to 607 MPa (~11 %) and ultimate compressive strength also decreased from 942 MPa to 745 MPa (~21 %). However, temperature enhancement caused increase of total strains about 15 % for the specimens owing to the softening effect. Sajadifar et al. (Sajadifar et al., 2013) studied deformation behavior of 4340 steel at temperatures between 900-1200 °C at strain rates from 0.01 to 1 $s^{-1}$. The yield strengths determined in that study was lower compared to the strengths in current study owing to higher temperature effect.

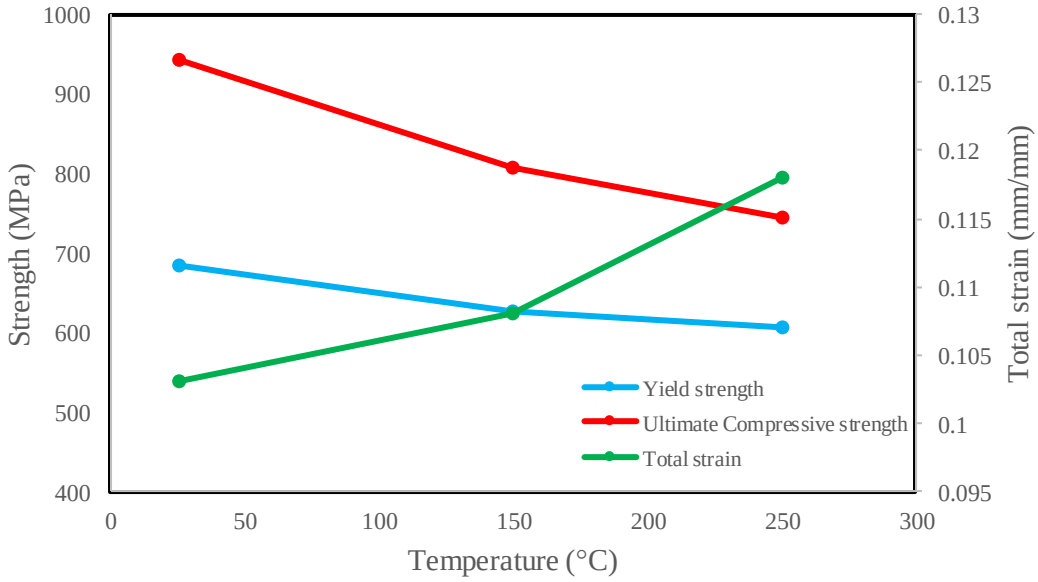


**Figure 7.** The change of strengths and total strains with temperature.

*4.1.3.Taylor impact test results*

In Table 1, final dimensions and deformation modes of the impacted specimens after Taylor impact tests are presented. With the increase of impact velocity, final diameters increased whereas final lengths decreased owing to the extreme plastic deformations. The

increase in the diameters of the specimens from the lowest to highest impact velocities were obtained approximately 43 %, 79 % and 147 % respectively. The decrease of final lengths of the specimens were determined 15 %, 22 % and 33 % for the impact velocities of 245, 324 and 336 $ms^{-1}$ respectively. Different impact velocities caused different deformation modes for the specimens. At the lowest impact velocity, no crack initiation occurred at impact surface. However, for the highest impact velocity, shear cracks at direction of 45° occurred and at on-going deformation process fracture and finally fragmentation was formed around impact surface.

**Table 1.** Experimental results for Taylor impact tests.

| Specimen | Impact velocity (m/s) | Final diameter (mm) | Final length (mm) | Deformation mode |
|---|---|---|---|---|
| 1 | 245 | 11.4 | 20.5 | Mushrooming |
| 2 | 324 | 14.3 | 18.7 | Shear crack |
| 3 | 336 | 19.8 | 16.0 | Shear crack + Fracture |

Figure 8 illustrates the final specimens after deformation due to impact with different velocities. As can be seen from the image, all specimens possessed mushroomed-like shape after impact. As the impact velocity increased, final length of the specimens decreased whereas final diameters increased. The impact velocity of 245 $ms^{-1}$ did not lead any crack initiation at the impact surface of the specimen. However, increase of velocity impact from 245 $ms^{-1}$ to 324 $ms^{-1}$ led to initiation of small shear cracks at the impact surface of the specimen and larger shear cracks and fracture for the specimen with impact velocity of 336 $ms^{-1}$. In a study by Kumar and Dixt (Kumar and Dixt, 2017), fracture behavior of steel rod specimen was investigated by simulation studies and the results were compared with test results. They declared that no fracture occurred at the impact surface of the specimen with impact velocity of 250 $ms^{-1}$. Only mushrooming deformation was observed for that specimen. However, as the impact velocity increased from 250 $ms^{-1}$ to 350 $ms^{-1}$, at the initial stage of impact mushrooming deformation occurred and at the end of deformation process shear cracks occurred at the impact surface. The deformation characteristics of the specimens with different velocities given in the current study is compatible with the results reported by Kumar and Dixt.

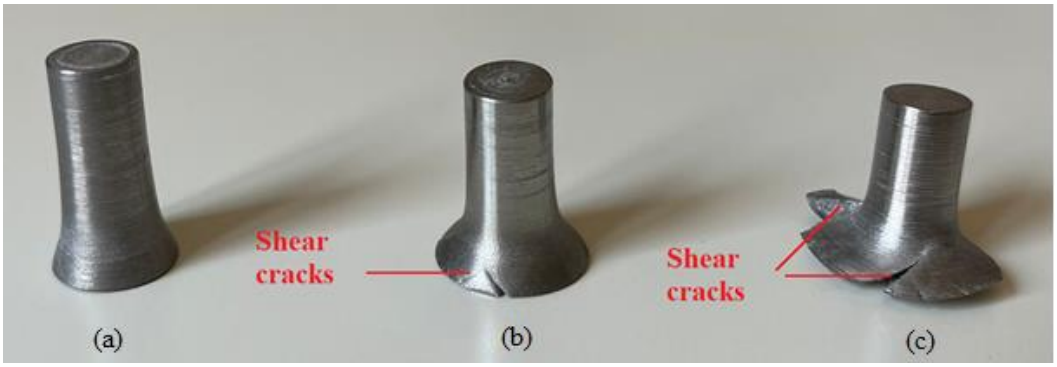


**Figure 8.** Deformed specimens after impact with three impact velocities **(a)** V=245 $ms^{-1}$ **(b)** V=324 $ms^{-1}$ **(c)** V=336 $ms^{-1}$.

### 4.2 Numerical Results

*4.2.1.Determination of Johnson-Cook strength model parameters*

Johnson-Cook strength model parameters of AISI 4340 steel in the current study were calculated by using the data obtained from quasistatic tensile tests and dynamic compression tests at both conditions of room and elevated temperatures. Johnson-Cook damage model parameters used in the simulations were taken from the reference (Johnson and Cook, 1985).

*Determination of A, B and n parameters*

In order to determine A, B and n parameters, quasi-static tensile tests at reference strain rate and reference temperature were specified as 0.1 $s^{-1}$ and 298 K respectively. Eq (4) can be modified as,

$$\sigma = [A + B\varepsilon^{n}] \tag{7}$$

The parameters at reference strain rate and reference temperature were determined by curve fitting method to the plastic region of quasistatic tensile test at reference strain rate and temperature (0.1 $s^{-1}$ and 298 K). According to that method, A, B and n parameters were obtained 577 MPa, 748 MPa and 0.293 respectively.

*4.2.2.Determination of C parameter*

The parameter C was determined by using quasi-static tensile tests at 0.001, 0.01, 0.1 $s^{-1}$ and dynamic compression tests at 725, 1500 and 2000 $s^{-1}$ These tests were performed at room temperature to eliminate the temperature parameter. According to the test conditions Eq (4) can be modified as,

$$\sigma = \left[A + B{\varepsilon_p}^n\right]\left[1 + C\ln\left(\frac{\dot{\varepsilon}}{\dot{\varepsilon}_0}\right)\right] \quad (8)$$

A curve- fitting approach involving nonlinear regression to the stress values at plastic strain of 0.04 at different strain rate conditions in the form of $\ln\left(\frac{\dot{\varepsilon}}{\dot{\varepsilon}_0}\right)$ (for *x* axis) - $\frac{\sigma}{[A+B{\varepsilon_p}^n]} - 1$ (for *y* axis) was employed. According to the data, parameter C was computed as 0.0078.

*4.2.3.Determination of m parameter*

To calculate m parameter, the stress values (at plastic strain of 0.04) from totally three different temperatures (two elevated temperatures of 150 °C and 250 °C and room temperature) at strain rate of 725 $s^{-1}$ were used. By putting the parameters A, B, n and C in Eq. (4) and applying a nonlinear curve fitting process, the parameter m was obtained to be 0.92.

The parameters calculated by curve fitting to the test data mentioned above are given in Table 2.

**Table 2.** Johnson-Cook material model parameters.

| A (MPa) | B (MPa) | n | C | m | D1 | D2 | D3 | D4 | D5 |
|---|---|---|---|---|---|---|---|---|---|
| 577 | 748 | 0.293 | 0.0078 | 0.92 | 0.05 | 3.44 | -2.12 | 0.002 | 0.61 |

*4.2.4.Mesh dependency*

The change of final lengths of the impacted specimen with element size is given in Figure 9. The final lengths were compared between each other for each element size. As can be seen from the figure, as the element size decreased, a convergence in the final lengths was obtained at the element size of 0.5 x 0.5 x 0.5 $mm^3$.

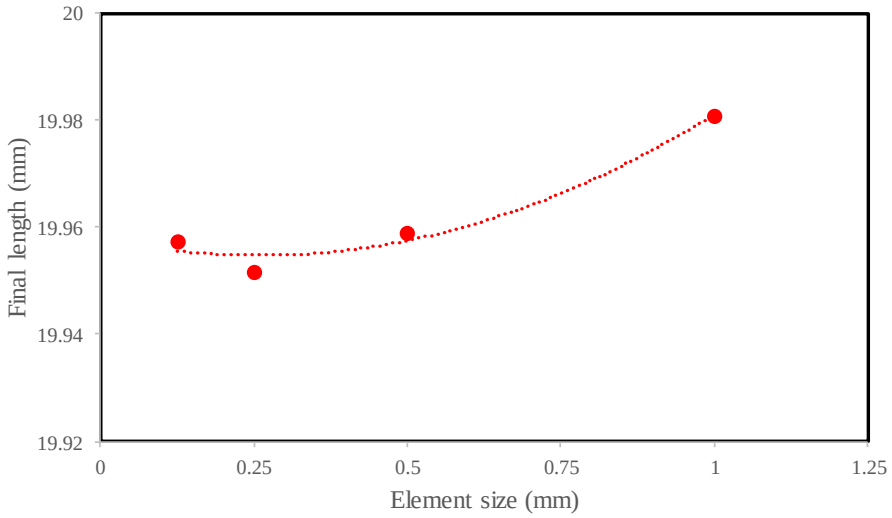


**Figure 9.** The change of final length of specimen with element size.

In addition to convergence study, CPU time is another significant parameter that should be considered for deciding the appropriate element size. As element size decreased from 1 x 1 x 1 $mm^3$ to 0.125 x 0.125 x 0.125 $mm^3$, the CPU time increased excessively from 263 seconds to 9464 seconds. Owing to mesh dependency results, element size of 0.25 x 0.25 x 0.25 $mm^3$ with a reasonable CPU time was chosen as the proper element size for the further Taylor impact analysis. The maximum aspect ratio and the characteristic length of the entire model with the element size of 0.25 x 0.25 x 0.25 $mm^3$ for specimen and 0.5 × 0.5 × 0.5 $mm^3$ for target were obtained as 2.26 and 0.5 mm respectively. The illustration of chosen FEM model after mesh dependency studies is given in Figure 10.

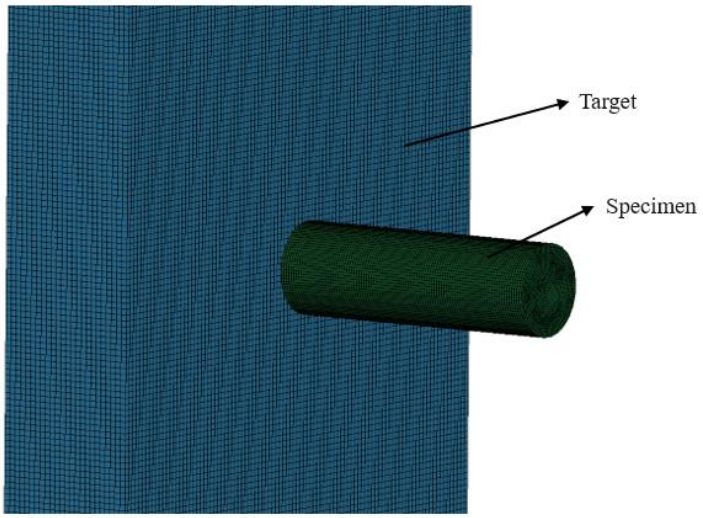


**Figure 10.** FEM Model used for Taylor Impact Test Simulations After Mesh Dependency.

*4.2.5.Taylor impact analysis*

Figure 11 indicates the comparison of simulated and tested specimens for three impact velocities. In this figure, optically scanned test specimens were given for comparison. Reasonable results were obtained in terms of final deformation geometries for both simulation and test results. Specimens comprise two distinct regions as shown in Figure 11 (a). Region around impact surface is the most heavily deformed region due to the flow of the material radially. As going further from the impact surface, there is a less deformed region before reaching to undeformed region. Undeformed region is the elastically deformed part of the specimen far from the impact surface.

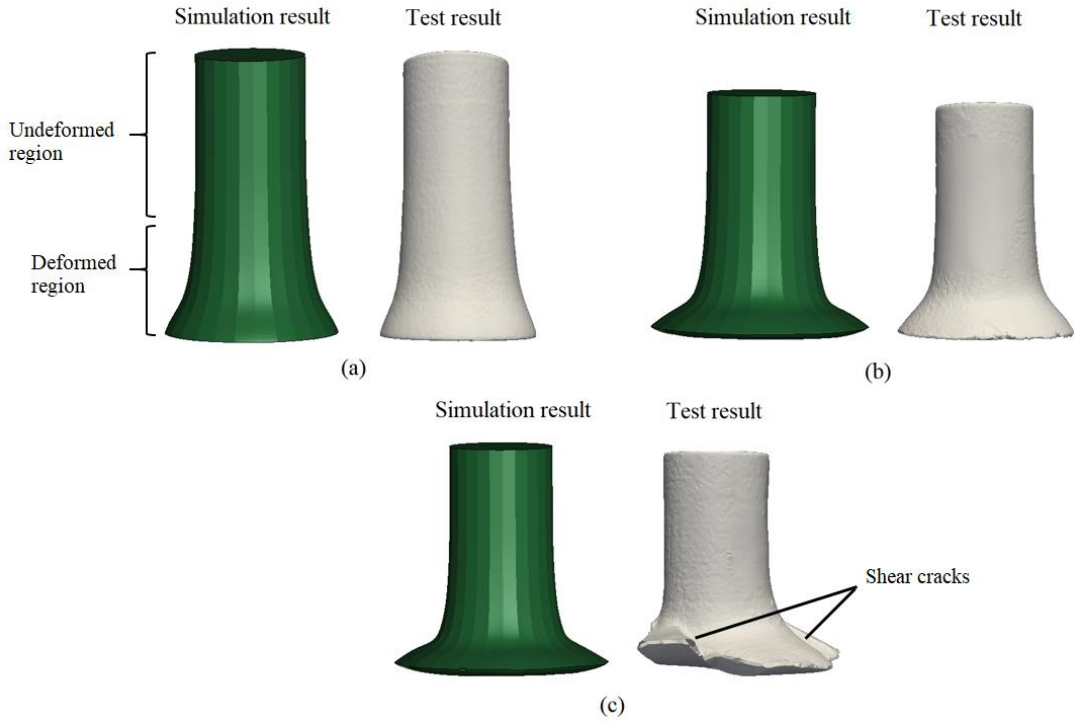


**Figure 11.** Comparison of simulated and tested specimens **(a)** V=245 $ms^{-1}$ **(b)** V=324 $ms^{-1}$ **(c)** V=336 $ms^{-1}$.

Strain rates obtained from the elements at four different locations along the cross-section of the deformed specimens are shown in Figure 12. The graph indicates that the maximum strain rates with the order of $10^5$ were determined at the impact surface due to extreme plastic deformation. As going further from impact surfaces towards undeformed regions, strain rates tended to decrease from the order of $10^5$ to the order of $10^3$. At the element located near the upper surface (point #1), strain rates were obtained 0 $s^{-1}$ for the specimens with the impact velocities of 245 and 324 $ms^{-1}$. For the specimen with impact velocity of 336 $ms^{-1}$, strain rate with the order of $10^2$ was obtained for point #1. These strain rate orders determined from numerical studies are consistent with reported strain rates in the literature (Martin et al., 2008).

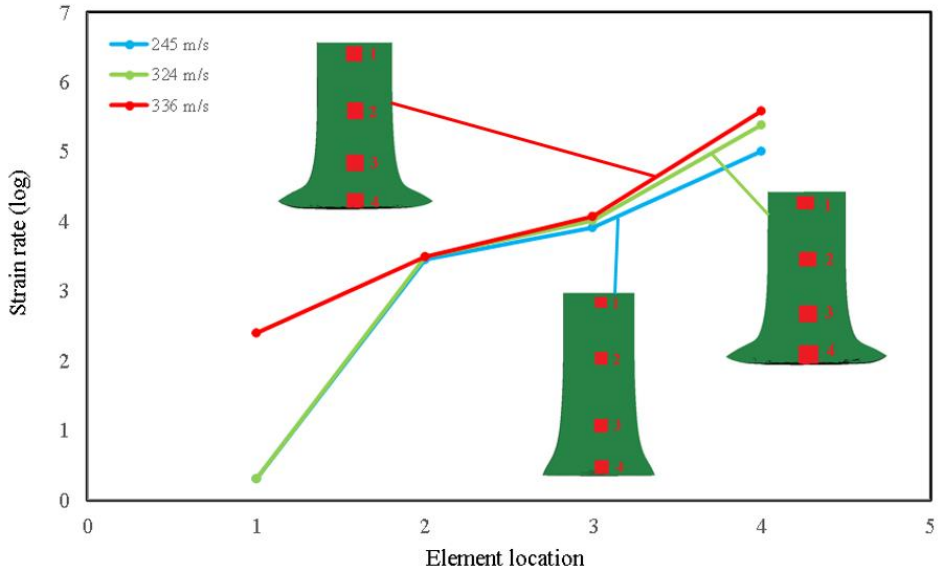


**Figure 12.** Strain rates obtained at four different locations at cross-sections of deformed specimens.

Temperature change contours along the cross-section of Taylor impact test specimens for three impact velocities are shown in Figure 13. The figure indicates that the impact surface of the specimen exhibited higher temperatures due to higher plastic deformation compared to the other regions of the specimen. From impact surface to undeformed region, the temperature change decreased for all the specimens. The change of the temperature increased as the impact velocity increased. The maximum change in temperature increased from 537 °C to 1311 °C with the increase in impact velocity. These high temperatures were observed in local areas of deformed region of the specimen. It is evident that due to no plastic deformation in undeformed region, no temperature change was observed at the cross-section of the specimen (blue color). Kar et al. (Kar et al., 2020) simulated Taylor impact test at room temperature for various BCC metals. They investigated the temperature distribution for tantalum specimen after impact test. According to their results, the maximum temperatures for the specimens were obtained as 681 and 806 °C for the impact velocities 135 and 155 $ms^{-1}$ respectively. The variations in temperatures between their study and the current study can be due to difference in impact velocities and materials.

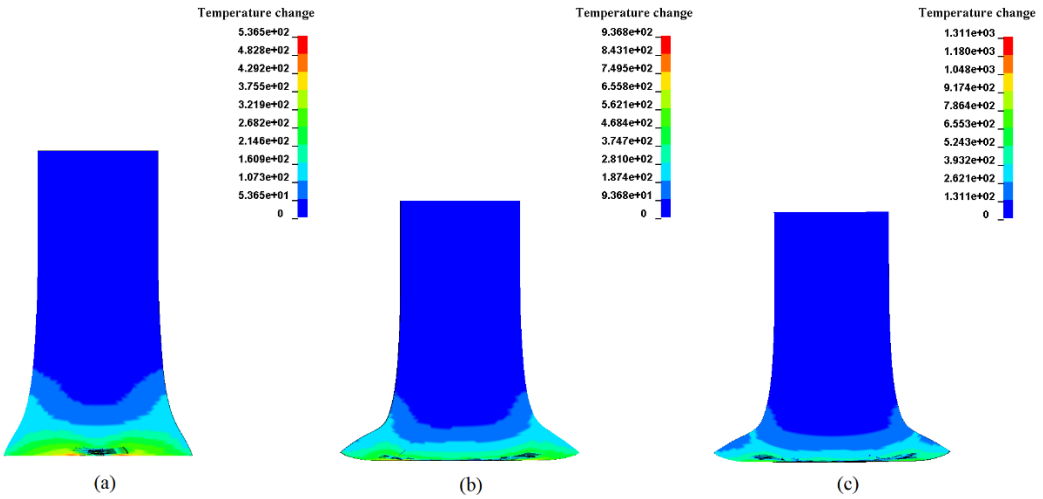


**Figure 13.** Temperature distribution contours at cross-section views of specimens **(a)** V=245 $ms^{-1}$ **(b)** V=324 $ms^{-1}$ **(c)** V=336 $ms^{-1}$.

The effective stress distribution at cross sections of the specimens for three impact velocities are shown in Figure 14. These contours were obtained at the moment when the impact velocities equaled to zero at impact process. The regions between impact surfaces and undeformed regions possessed higher stresses than the other regions. The increase of impact velocity led to increase of high stress area in that region (red color in cross-section view) and in the deformed region where material laterally moved due to high plastic deformation (Figure 14 (c), regions in blue dashed circles).

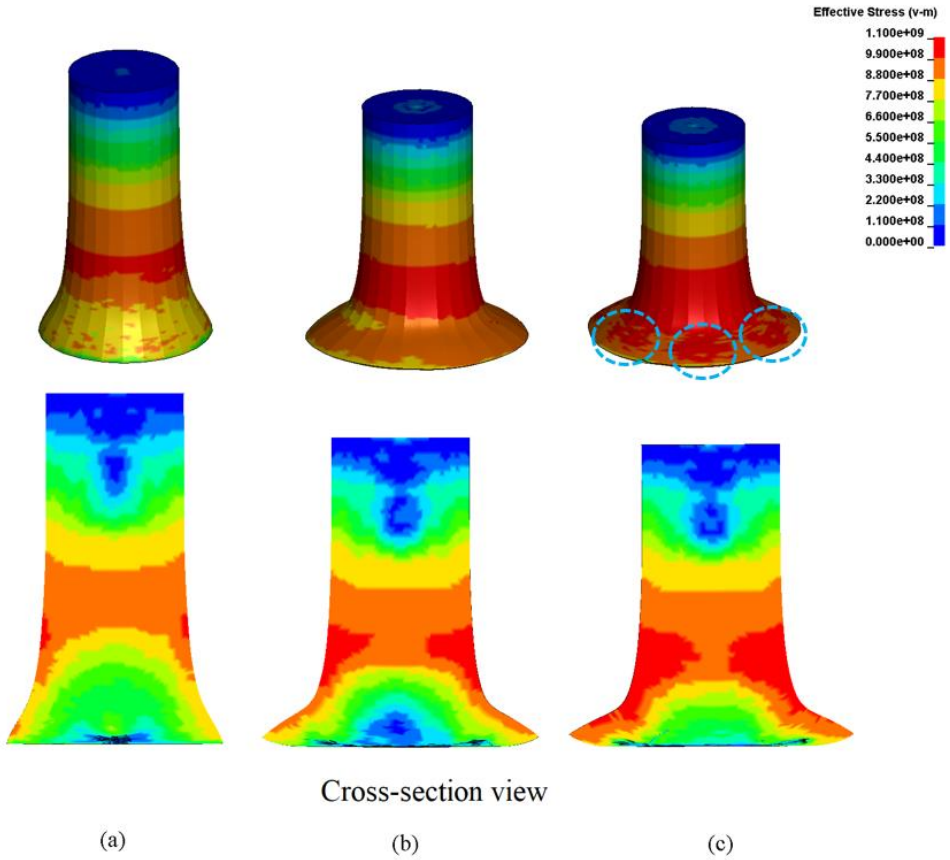


**Figure 14**. Effective stress distribution at cross-section views of specimens after impact **(a)** V=245 $ms^{-1}$ **(b)** V=324 $ms^{-1}$ **(c)** V=336 $ms^{-1}$.

In Figure 15, damage contours of the specimens with three impact velocities are illustrated. As can be seen from the figure, as the impact velocity increased, the damage generated at the region near impact surface raised especially at the maximum of the diameters of the impact surfaces. The high temperature change, high effective stress and damage accumulation near impact surfaces shown in Figure 13 (b)-(c), Figure 14 (b)-(c) and Figure 15 (b)-(c) in deformed region might lead to shear crack initiation and fracture located near impact surface (Figure 8). The higher temperature which was due to large plastic deformation might lead to softening of the material around that region which could cause cracking (Chen and Huang, 2016). In a study by Rakvag et al. (Rakvag et al., 2014), Arne tool steel specimens were impacted to rigid target with the velocities in the range of about 125-360 $ms^{-1}$. They reported that as the impact velocity was about 300 $ms^{-1}$ the specimens exhibited shear cracks at the impact surface.

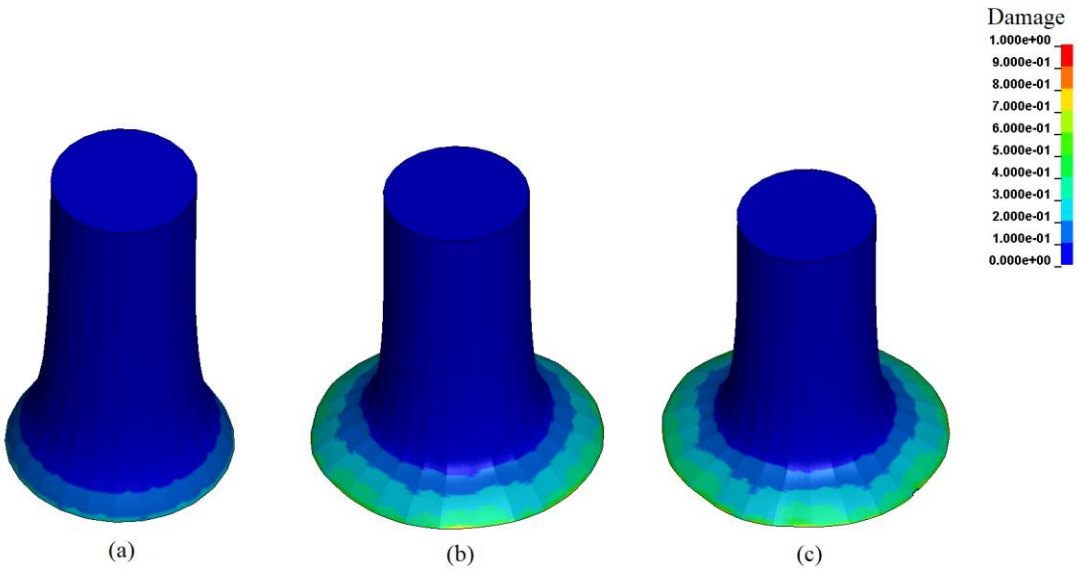


**Figure 15.** Damage contours of the specimens after impact **(a)** V=245 $ms^{-1}$ **(b)** V=324 $ms^{-1}$ **(c)** V=336 $ms^{-1}$.

In Figure 16, existing and disappearing of porosities at impact region during initial and final deformation process are shown at cross-sections of specimens. In this figure, the porosities in the center of the specimens are illustrated inside of red dashed circles. When the specimen initially impacts the target, compression waves travel laterally and reach the lateral free surface of the specimen and these compression waves transforms to tensile waves which travel back to the center of the specimen. When tensile waves reach to the center of the specimen and collide each other, they produce high tensile stress and high deformation zones which lead to nucleation of porosity (Campagne et al., 2008). This result is consistent with the result given in Campagne-Lambert et al. (Campagne et al., 2008). According to the results in Figure 16, as the impact velocity increased, the porosity volume created in the center of the specimen at initial stage of deformation also increased owing to the increase of stress. At the final stage of the deformation, these porosities disappeared owing to the excessive deformation.

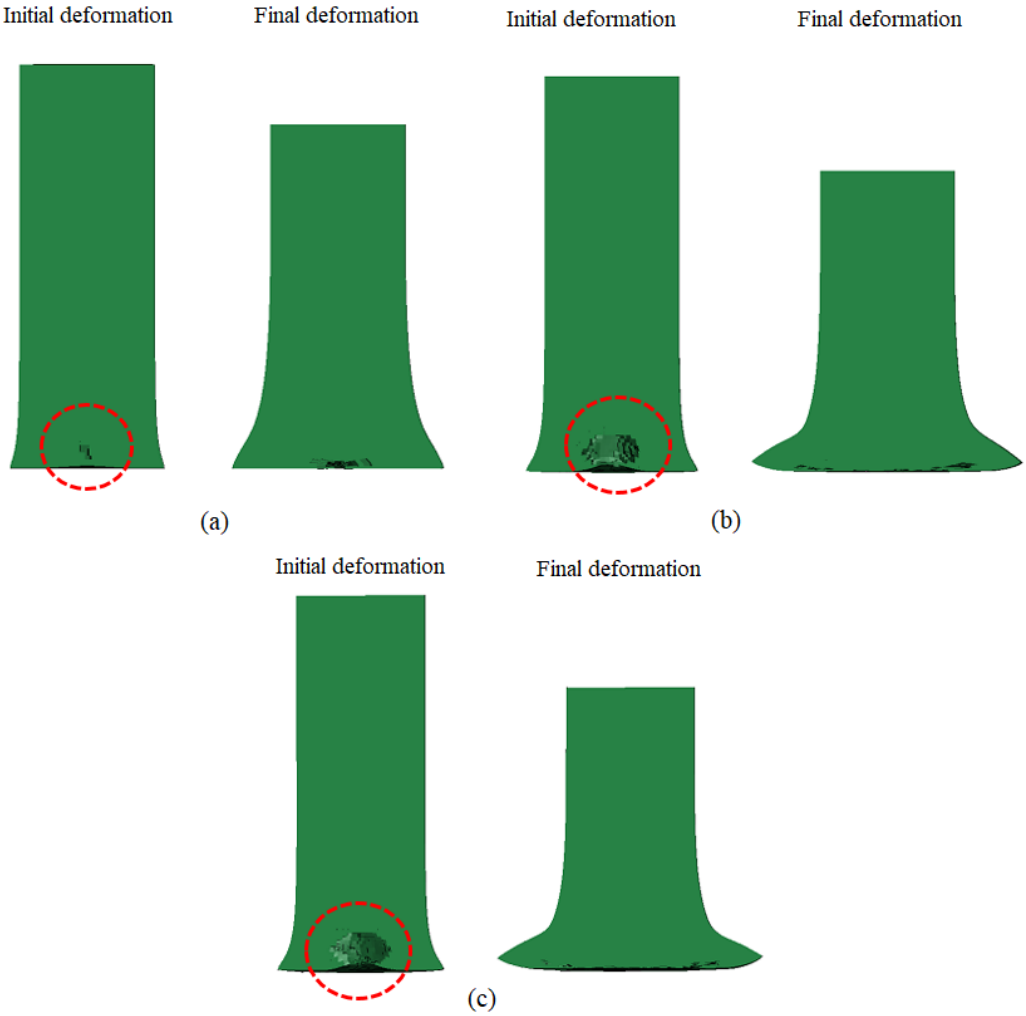


**Figure 16**. Porosity at cross-section views of specimens for initial and final deformations **(a)** V=245 $ms^{-1}$ **(b)** V=324 $ms^{-1}$ **(c)** V=336 $ms^{-1}$.

## 5. Conlusions

In this study, dynamic compression behavior of AISI 4340 steel was investigated by dynamic compression tests using split-Hopkinson pressure bar and Taylor impact tests. Test results were compared with numerical studies. The results are as follows.

- The increase of strain rate in compression tests from 725 to 2000 $s^{-1}$ led to increase of yield and ultimate strengths about 17 % and 14 % respectively. Total strain also increased about 146 % with the strain rate. Temperature increase at compression tests from room temperature to 250 °C diminished yield and ultimate strengths around 11 % and 21 % respectively. The high temperature enhanced total strains of the specimens about 15 % due to softening effect.
- Taylor impact test results showed that the specimen with impact velocity of 245 $ms^{-1}$ possessed only mushrooming deformation. As the impact velocity increased from 245 $ms^{-1}$ to 324 $ms^{-1}$ small shear cracks initiated around the impact surface. At the velocity of 336 $ms^{-1}$, larger shear cracks initiated and fracture occurred at the impact surface.
- Numerical results showed that highest temperature changes in the range of 537-1311 °C were obtained in local regions at impact surfaces of all impact conditions. In addition, the increase of impact velocity from 245 $ms^{-1}$ to 336 $ms^{-1}$ enhanced the effective stress distribution and damage accumulation at deformed region near impact surface especially for the specimen

impacted at 336 $ms^{-1}$. The fracture at impact surface of that specimen is a result of the high stress generated around impact surface.

**References**

Acosta C.A., Hernandez C., Maranon A., Casas-Rodriguez J.P. (2016). Validation of material constitutive parameters for the AISI 1010 steel from Taylor impact tests, Materials and Design, 2016, 110, 324-331.
ASTM E8, Standard test methods for tension testing of metallic materials, ASTM International.

Campagne L., Daridon L., Oussouaddi O., Ahzi S., Sun X. (2008). Simulation of the Taylor impact test and analysis of damage evolution using a nucleation and growth based approach, Modeling, Measurement and Control, 77 (3-4), 19-35.

Chakraborty S., Shaw A., Banerjee B. (2015). An axisymmetric model for Taylor impact test and estimation of metal plasticity, Proceedings of the Royal Society A: Mathematical, Physical and Engineering Sciences, 471(2174), 20140556.

Chen W., Song B. (2010). Split Hopkinson (Kolsky) Bar Design, Testing and Applications, Springer Science and Business Media.

Chen G., Huang X. (2016). Simulation of deformation and fracture characteristics of a 45 steel Taylor impact specimen, Engineering Transactions, 64(2), 225-240.

Johnson G.R., Cook W.H. (1983). A constitutive model and data for metalssubjected to large strains, high strain rates and high temperatures, Proceedings of the 7th International Symposium on Ballistics, 21, 541-7.

Johnson G.R., Cook W.H. (1985). Fracture characteristics of three metals subjected to various strains, strain rates, temperatures and pressures, Engineering Fracture Mechanics, 21(1), 31-48.

Kar G., Roy Chowdhury S., Roy D. (2020). A nonequilibrium thermodynamic model for viscoplacticity coupled with damage for BCC metals, Mechanics of Advanced Materials and Structures, 27(13), 1110-1119.

Kumar M., Dixt P.M. (2017). Simulation of Fracture in the Taylor Test Using Continuum Damage Mechanics Model. Procedia Engineering, 173, 1215-1222.

Martin M., Shen T., Thadhani N.N. (2008). Instrumented anvil-on-rod impact experiments for validating constitutive strength model for simulating transient dynamic deformation response of metals, Materials Science and Engineering: A, 494(1-2), 416-424.

Mehrabi A., Sharifi H., Asadabad M.A., Najafabadi R.A., Rajaee A. (2020). Improvement of AISI 4340 steel properties by intermediate quenching – microstructure, mechanical properties, and fractography, International Journal of Materials Research, 111(9), 711-779.

Odeshi A.G., Al-ameeri S., Mirfakhraei S., Yazdani F., Bassim M.N. (2006). Deformation and failure mechanism in AISI 4340 steel under ballistic impact, Theoretical and Applied Fracture Mechanics, 45, 18-24.

Odeshi A.G., Bassim M.N. (2009). High strain-ratefracture and failure of a high strength low alloy steel in compression, Materials Science and Engineering: A, 525(1-2), 96-101.

Odoh D., Owolabi G., Odshi A. (2013). Whitworth H, Shear Band Formation in AISI 4340 Steel Under Dynamic Impact Loads: Modeling and Experiment, Acta Metallurgica Sinica (English Letters), Vol:26, No:4, 378-384.

Owolabi G., Odoh D., Odeshi A., Whitworth H. (2013). Occurrence of Dynamic Shear Bands in AISI 4340 Steel under Impact Loads, World Journal of Mechanics, 3, 139-145.

Piao M., Huh H., Lee I., Ahn K., Kim H., Park L. (2016). Characterization of flow stress at ultra-high strain rates by proper extrapolation with Taylor impact tests, International Journal of Impact Engineering, 91, 142-157.

Rakvag K.G., Borvik T., Hopperstad O.S. (2014). A numerical study on the deformation and fracture modes of steel projectiles during Taylor bar impact tests. International Journal of Solids and Structures, 51(3-4), 808-821.

Ramesh K.T. (2008). High Strain Rate and Impact Experiments, Springer Handbook of Experimental Solid Mechanics, J. Sharpe, W. N., Editor. Springer.

Sajadifar S.V., Yapici G.G., Ketabchi M., Bemanizadeh B. (2013). High temperature deformation Behavior of 4340 steel:activation energy calculation and modeling of flow response, Journal of Iron and Steel Research International, 20(12), 133-139.

Sen S., Banerjee B., Shaw A. (2020). Taylor impact test revisited: Determination of plasticity parameters for metals at high strain rate, International Journal of Solids and Structures, 193-194, 357-374.

Souza M.F., Serrao L.F., Pardal J.M., Tavares S.S.M., Fonseca M.C. (2022). Tempering influence on residual stresses and mechanical properties of AISI 4340 steel, The International Journal of Advanced Manufacturing Technology, 120:1123-1134.

Teng X., Wierzbicki T., Hiermaier S., Rohr I. (2005). Numerical prediction of fracture in the Taylor test. International Journal of Solids and Structures, 42(9-10), 2929-2948.

Xiao X.K., Zhang W., Wei G., Mu Z.C. (2010). Effect of projectile hardness on deformation and fracture behavior in the Taylor impact test, Materials & Design, 31(10), 4913-4920.